



ELSEVIER

Contents lists available at [ScienceDirect](https://www.sciencedirect.com)

Journal of Sound and Vibration

journal homepage: www.elsevier.com/locate/jsvi

Duct sound produced by vortex flow over a splitter plate

S.K. Tang

School of Engineering, The University of Hull, Hull HU6 7RX, United Kingdom

ARTICLE INFO

*Keywords:*Vortex sound
Duct
Scattering

ABSTRACT

This paper examines the sound generated by an inviscid low Mach number vortex filament as it moves near a semi-infinite splitter in a two-dimensional duct with and without vortex shedding at the splitter edge. A strong one-dimensional sound is produced when the vortex is close to the edge. Without vortex shedding, the sound is shown to consist of predominantly compressive pulses which propagate in the split duct section and a rarefaction pulse downstream of the splitter edge, regardless of the position of the half plate and the direction of vortex motion. The vortex shedding results in no horizontal force at and no sound going downstream of the edge. Results also suggest that the vortex shedding does not always result in noise reduction. In all cases with and without vortex shedding, the narrower section of the split duct experiences the most sound in general. The surprising result is found that the confinement of the edge-scattering flow within a duct does not much affect the high acoustic efficiency of the scattering process.

1. Introduction

Howe's Theory of Vortex Sound [1] gives a comprehensive account of why aerodynamic sound is produced more effectively when unsteady flow interacts with solid surfaces. This paper is motivated by a desire to know whether the same is true when the flow is contained within ducts of the kind found in air-conditioning systems.

The inviscid scattering theories developed by Ffowcs Williams and Hall [2] and Crighton and Leppington [3] indicate that a strong sound with distinct directional characteristics results from the interaction of unsteady high Reynolds number flow with sharp baffle edges. Crighton [4] and Cannell and Ffowcs Williams [5] used simple vortex filament problems to estimate aeroacoustic details and to demonstrate that edge-scattering is a much more effective way of making sound than is free vorticity. Howe [1] also discussed this strong sound scattering process of vorticity negotiating an edge in unbound medium using a Green's function approach.

Low Mach number flows inside air-conditioning ducts are often turbulent and noisy. Davies and Ffowcs Williams [6] demonstrated that confinement of turbulence within a duct increases the flow's ability to make sound. Confinement and edge-scattering both increase the noise of turbulence. Sharp-edged panels are found in air conditioning systems whenever ducts fork and flows merge. These features would be expected to be noisy, judging by their scattering ability in open space and one wonders whether their confinement within a duct might not further increase their acoustic significance. This paper considers that issue by solving a simple related example.

We generalize Crighton's problem of inviscid vortex flow negotiating the edge of a half-plane, by including the effect of confinement within a duct. This definite example of edge scattering within a hard-walled duct is of course a drastic oversimplification of real flows, but we think that the example is generic enough that its detailed solution might provide useful pointers for understanding practical cases of flow noise, as did Crighton's original problem [4]. The usefulness of our inviscid analysis is fully justified by the prominent place it has attracted in major reviews of the subject and by comparison with experiment (for instance, Crighton [7]). There

E-mail address: S.Tang@hull.ac.uk.

<https://doi.org/10.1016/j.jsv.2022.117352>

Received 28 March 2022; Received in revised form 17 September 2022; Accepted 30 September 2022

Available online 5 October 2022

0022-460X/© 2022 The Author. Published by Elsevier Ltd. This is an open access article under the CC BY-NC-ND license (<http://creativecommons.org/licenses/by-nc-nd/4.0/>).

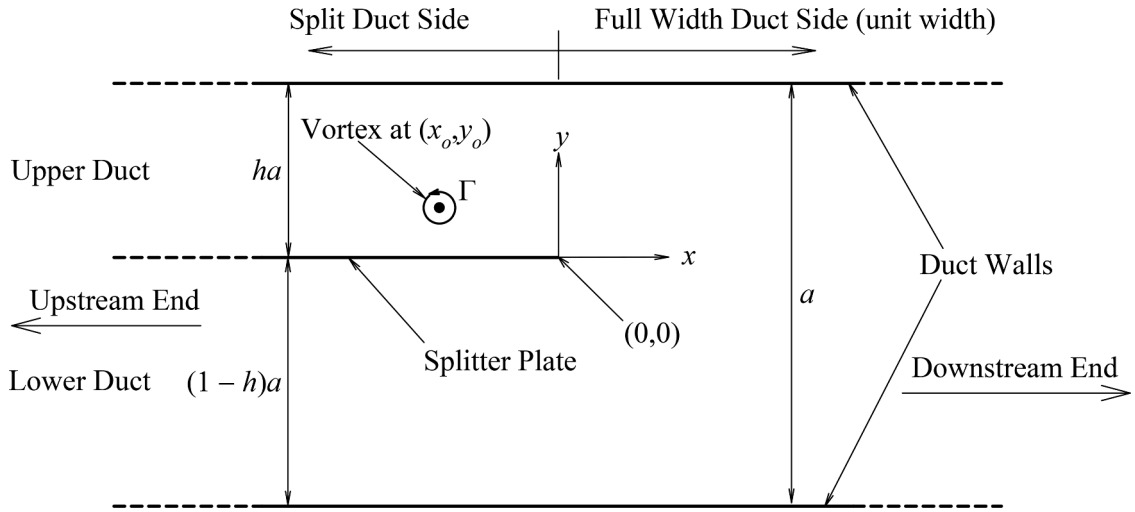


Fig. 1. Schematic diagram of the vortex-duct system.

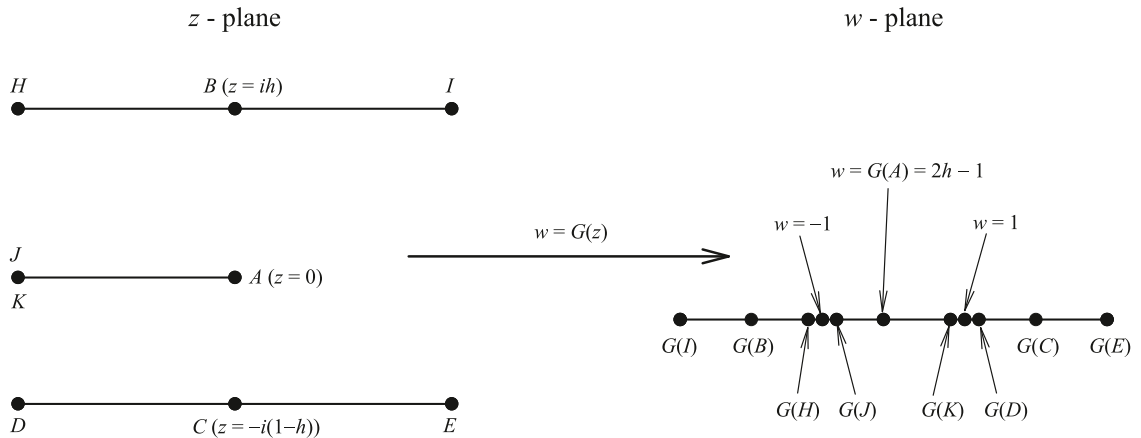


Fig. 2. Conformal mapping between z-plane and w-plane.

are also more recent studies using inviscid vortex analogy to get insights into the aeroacoustics of vortex-induced flows with and without rigid scattering edges (for instance, Howe [8], Manela and Huang [9] and Abou-Hussein et al. [10]). In addition, the use of inviscid incompressible approximation helps develop analytical solution which enables the analysis of various scaling in the sound power radiation process of a vortex negotiating a scattering edge confined within a duct. It also provides the required analytical incompressible flow field far away from the edge, facilitating the use of matched asymptotic expansion for far field sound estimation.

The present study is commenced without imposing Kutta condition [11] at the splitter edge. The second part of this paper investigates the effect of vortex shedding on the vortex motions and the overall sound radiation.

2. Without vortex shedding

2.1. Vortex paths

Fig. 1 illustrates the present ‘splitter-plate-in-a-duct’ system. The duct is two-dimensional and is infinitely long. The splitter is parallel to the duct walls, dividing the duct of unit height into two smaller ducts in the region $x < 0$. The sharp splitter edge is chosen as the origin of the two dimensional co-ordinate system. Γ denotes the circulation of the vortex and $z_o = (x_o, y_o)$ the position of the vortex which is time dependent. The relative position of the splitter-plate inside the duct is represented by the height factor h . All the length scales in this study are normalized by the width of the main duct, a . Without loss of generality, we set $a = 1$.

The complex velocity potential representing the incompressible vortex-induced near-field in this geometry can be obtained by conformal mapping. The transformation that maps the upper complex half-plane w to the present complex $z (= x + iy)$ plane, (c.f. Churchill and Brown [12]), can be written as

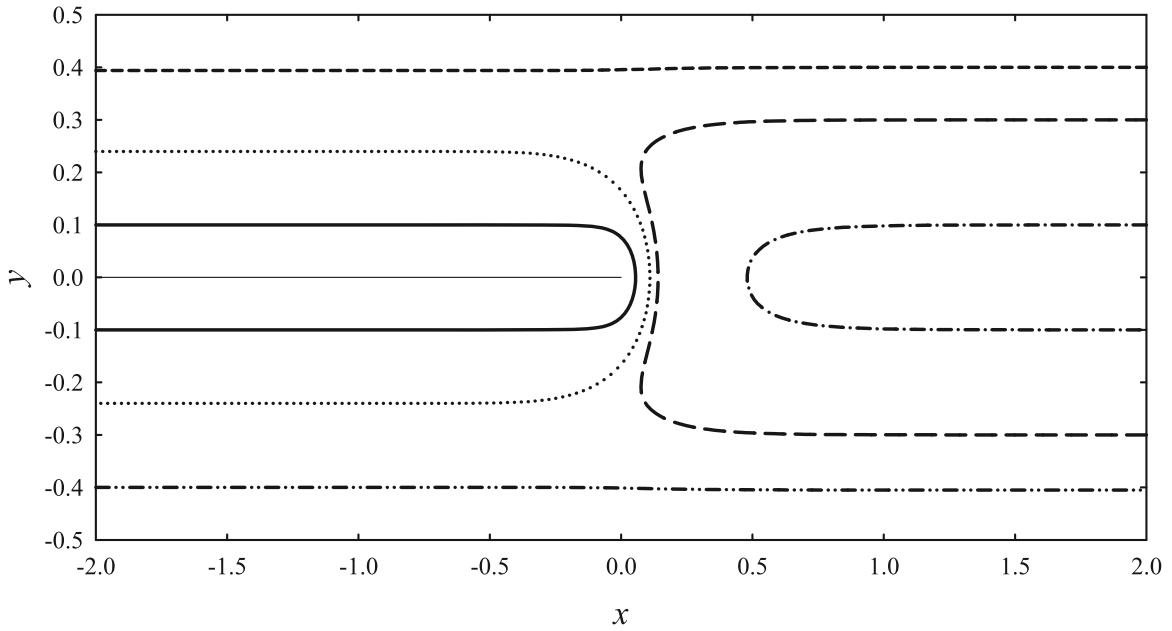


Fig. 3. Vortex flight paths for $h = 0.5$: $y_i = \pm 0.1, x_i < 0, \Gamma = \pm 1$; $\cdots \cdots \cdots$: $y_i = \pm 0.24, x_i < 0, \Gamma = \pm 1$; $\cdots \cdots \cdots$: $y_i = \pm 0.1, x_i > 0, \Gamma = \pm 1$; $---$: $y_i = 0.4, x_i > 0, \Gamma = -1$; $\cdots \cdots \cdots$: $y_i = -0.4, x_i < 0, \Gamma = 1$; $\cdots \cdots \cdots$: $y_i = \pm 0.3, x_i > 0, \Gamma = \pm 1$; thin solid line represents the splitter plate.

$$z = \frac{1}{\pi} \left\{ h \ln(w+1) + (1-h) \ln(w-1) - h \ln\left(\frac{h}{1-h}\right) - \ln[2(1-h)] - i(1-h)\pi \right\} = F(w). \tag{1}$$

Fig. 2 illustrates the two complex planes involved. We denote the inverse transform as $G \equiv F^{-1}$ so that $w = G(z)$. The complex potential Ω produced by a vortex, together with its image in the real axis of the w plane, is

$$\Omega = \phi + i\psi = -\frac{i\Gamma}{2\pi} \ln \left[\frac{G(z) - G(z_0)}{G(z) - \overline{G(z_0)}} \right] + \gamma, \tag{2}$$

where the bar denoting a complex conjugate and γ a sole function of time. γ is included here as a general solution of the incompressible flow potential. The fluid velocity at a point z , is

$$u - iv = \frac{d\Omega}{dz} = -\frac{i\Gamma}{2\pi} \left[\frac{1}{G(z) - G(z_0)} - \frac{1}{G(z) - \overline{G(z_0)}} \right] G'(z), \tag{3}$$

where ' denotes a differentiation with respect to z . Substituting $z = z_0 + \epsilon$ in Eq. (3), one obtains, for very small ϵ , that

$$\frac{d\Omega}{dz} \Big|_{z=z_0+\epsilon} = -\frac{i\Gamma}{2\pi} \left[\frac{1}{G(z_0 + \epsilon) - G(z_0)} - \frac{1}{G(z_0 + \epsilon) - \overline{G(z_0)}} \right] G'(z_0 + \epsilon). \tag{4}$$

The application of Taylor's expansion to G at z_0 gives

$$\frac{d\Omega}{dz} \Big|_{z=z_0+\epsilon} = -\frac{i\Gamma}{2\pi} \left[\frac{1}{\epsilon} + \frac{G''(z_0)}{2G'(z_0)} - \frac{G'(z_0)}{G(z_0) - \overline{G(z_0)}} \right] + O(\epsilon). \tag{5}$$

Since the term with $1/\epsilon$ is the velocity field induced by the vortex in free space and does not act on the vortex itself, the vortex moves with the complex velocity which is the finite part of this expression as $\epsilon \rightarrow 0$:

$$\frac{dx_0}{dt} + i \frac{dy_0}{dt} = \frac{i\Gamma}{2\pi} \left[\frac{G''(z_0)}{2G'(z_0)} - \frac{G'(z_0)}{G(z_0) - \overline{G(z_0)}} \right]. \tag{6}$$

The flight path of the vortex can be obtained once G is known and the initial position of the vortex, $z_i (= x_i + iy_i)$, is specified, by carrying out a time integration of $\partial x_0/\partial t + i \partial y_0/\partial t$; we do this using the fourth order Runge-Kutta method with adaptive step size control.

The inverse transform function G , in general, has to be evaluated numerically, but it takes simple forms for some values of h . For instance when $h = 0.5$,

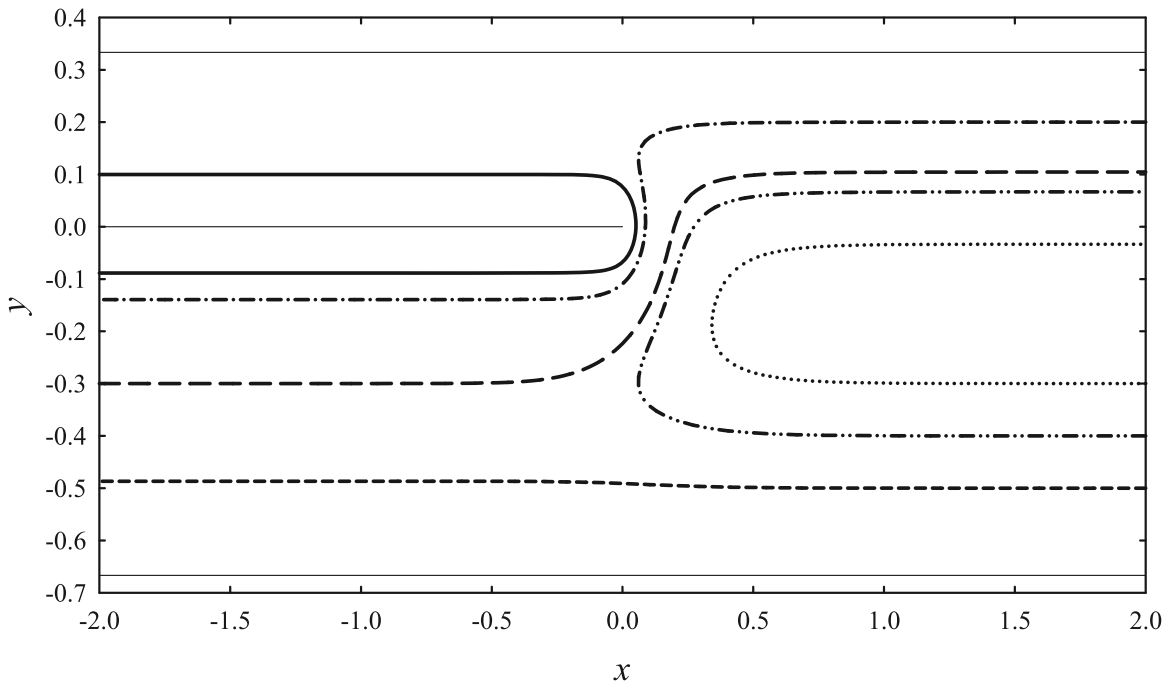


Fig. 4. Vortex flight paths for $h = 1/3$: $y_i = 0.1, x_i < 0, \Gamma = 1$; $\dots\dots\dots$: $y_i/a = -0.3, x_i > 0, \Gamma = -1$; $\dashdot\dashdot\dashdot$: $y_i = 0.2, x_i > 0, \Gamma = 1$; $-\ - - -$: $y_i = -0.5, x_i > 0, \Gamma = -1$; $\dots\dots\dots$: $y_i = -0.4, x_i > 0, \Gamma = -1$; $\dashdot\dashdot\dashdot$: $y_i = -0.3, x_i < 0, \Gamma = -1$; thin solid lines represent the splitter plate and the duct walls.

$$w = G(z) = \sqrt{1 - e^{2\pi z}} \text{ and } z = F(w) = \frac{1}{2\pi} \ln(1 - w^2). \tag{7}$$

Fig. 3 shows the essential features of the corresponding vortex trajectories with various initial vortex position z_i obtained after time integration of the vortex velocities for $h = 0.5$. The initial vortex position is far upstream (or downstream) of the edge. When the initial position of the vortex (of the right sign of circulation) is closer to the splitter plate than it is to the nearest duct wall, the vortex propagates towards the edge, then turns around the edge and finally propagates back on the other side. The corresponding flight path is symmetrical about $y = 0$. For $y_i \approx 0.25$, the initial speed of the vortex is infinitesimal. When $0.25 < y_i < 0.5$, the vortex with $\Gamma > 0$ eventually propagates slowly away from the edge. If $\Gamma < 0$, the vortex moves away from the edge for $0 < y_i < 0.25$, but will continue its propagation direction with a slight change in y_o for $0.25 < y_i < 0.5$.

When the vortex is initially located in the full-width duct, the vortex will move towards the edge of the half plane if $\Gamma > 0$ (anticlockwise circulation) and $0 < y_i \leq 0.33$. Some examples of its path are shown in Fig. 3. When it is sufficiently close to the edge region, it turns back and returns in the lower half plane. The vortex flight path is again symmetrical about the x -axis. For $0.33 < y_i < 0.5$, the vortex propagates past the edge if $\Gamma > 0$.

For $h = 0.5$, the vortex with an initial position z_i will have a flight path which is the mirror image of that with an initial position \bar{z}_i about the x -axis provided that the sign of the circulation is right. It can be noted that there is a relatively large change in the velocity of the vortex when it passes over the edge ($x_o \sim 0$); one would expect a high radiation of sound to be produced at and close to this instant.

When the half plate is offset, the vortex paths are no longer symmetrical about the x -axis. For $h = 1/3$, we find that

$$G(z) = \frac{2}{3} \left[2e^{3\pi z} \left(1 + \sqrt{1 - e^{-3\pi z}} \right) - 1 \right]^{\frac{1}{3}} + \frac{2}{3} \left[2e^{3\pi z} \left(1 + \sqrt{1 - e^{-3\pi z}} \right) - 1 \right]^{-\frac{1}{3}} + \frac{1}{3}, \tag{8}$$

and give some examples of the vortex flight paths in Fig. 4. For $y_i > 0$ and the initial vortex position is in the split duct, the vortex motions are similar to those in the symmetric case ($h = 0.5$) except that the vortex path is now not symmetrical about the splitter plate. For $y_i < 0$ and an initial vortex with anticlockwise circulation in the full-width duct, the vortex will turn around near the edge, but only for a limited y_i range. For initial vortex position in the split duct, the vortex with the right sense of circulation approaches the edge and then turns back as in the $h = 0.5$ case. Though there are some similarities between the vortex paths in the $h = 0.5$ and $h = 1/3$ cases, Fig. 4 shows that, for $h = 1/3$, a vortex with anticlockwise circulation initially propagating in the $y > 0$ range can pass across the edge and then continue its progress, but in the lower part of the split duct. That behaviour is never observed in the $h = 0.5$ case.

2.2. The incompressible flow far field

One can deduce from the mapping function Eq. (1) that as $x \rightarrow +\infty$,

$$z \approx \frac{\ln(w)}{\pi} - i(1-h) - h \ln\left(\frac{h}{1-h}\right) - \ln[2(1-h)] \Rightarrow w = G(z) \approx \beta e^{i(1-h)\pi} e^{\pi z}, \tag{9}$$

where $\beta = 2h^h(1-h)^{(1-h)}$. Therefore, $|w| = |G(z)| \rightarrow \infty$ so that $|G(z)| \gg |G(z_0)|$ at large distance downstream from the edge of the splitter plate regardless of the value of h . Also, the outer asymptotic solution of the inner incompressible flow field must match with that of a planar propagating wave. As we consider the present low Mach number vortex flow field is slightly compressible, it is necessary to include a planar fluid motion potential Vz in duct section far away from the splitter edge [5]. The corresponding velocity potential can then be expressed as

$$\Omega = -\frac{i\Gamma}{2\pi} \ln\left[\frac{G(z) - G(z_0)}{G(z) - \overline{G(z_0)}}\right] + \gamma + Vz = -\frac{i\Gamma}{2\pi} \ln\left[\left(1 - \frac{G(z_0)}{G(z)}\right) \sum_{j=0}^{\infty} \left(\frac{\overline{G(z_0)}}{G(z)}\right)^j\right] + \gamma + Vz = -\frac{\Gamma}{\pi} \frac{\text{Im}[G(z_0)]}{\beta e^{i(1-h)\pi} e^{\pi z}} + O\left(\left|\frac{G(z_0)}{G(z)}\right|^2\right) + \gamma + Vz, \tag{10}$$

and V is related to the magnitude of the far field plane wave downstream. One obtains

$$\phi_{x \rightarrow +\infty} \approx -\frac{\Gamma}{\pi\beta} \text{Im}[G(z_0)] e^{-\pi x} \cos[(h-1-y)\pi] + \gamma + Vx, \tag{11}$$

The first term on the right-hand-side of Eq. (11) decays exponentially with x and vanishes as $x \rightarrow +\infty$ regardless of the value of h . The sound far downstream of the splitter plate in the duct depends only on γ as V and γ are related (shown later).

One can observe from Eq. (1), which is also illustrated in Fig. 2, that as $x \rightarrow -\infty$, $w \rightarrow 1$ for $y < 0$ and $w \rightarrow -1$ for $y > 0$. The velocity potential there tends to be independent of x and y so there is no motion of the fluid far upstream. The outer asymptotic value of the potential near field in the split duct for $y < 0$, $x \rightarrow -\infty$, $\phi_{-\infty}^-$, is

$$\phi_{-\infty}^- \approx \text{Re}\left[-\frac{i\Gamma}{2\pi} \ln\left(\frac{1-G(z_0)}{1-\overline{G(z_0)}}\right)\right] + \gamma + V_{-\infty}^- x, \tag{12}$$

while that for $y > 0$, $x \rightarrow -\infty$, $\phi_{-\infty}^+$, is

$$\phi_{-\infty}^+ \approx \text{Re}\left[-\frac{i\Gamma}{2\pi} \ln\left(\frac{1+G(z_0)}{1+\overline{G(z_0)}}\right)\right] + \gamma + V_{-\infty}^+ x. \tag{13}$$

As the velocity potentials in Eqs. (11)–(13) must match with those of the far field propagating plane waves, it is straight-forward to show that

$$V = -\frac{1}{c} \frac{\partial \gamma}{\partial t}, \quad V_{-\infty}^+ = \frac{1}{c} \frac{\partial}{\partial t} \left\{ \text{Re}\left[-\frac{i\Gamma}{2\pi} \ln\left(\frac{1+G(z_0)}{1+\overline{G(z_0)}}\right)\right] + \gamma \right\} \text{ and } V_{-\infty}^- = \frac{1}{c} \frac{\partial}{\partial t} \left\{ \text{Re}\left[-\frac{i\Gamma}{2\pi} \ln\left(\frac{1-G(z_0)}{1-\overline{G(z_0)}}\right)\right] + \gamma \right\}. \tag{14}$$

Details of the derivation is given in Appendix A. For the incompressible far field, flow continuity requires that

$$V = hV_{-\infty}^+ + (1-h)V_{-\infty}^-, \tag{15}$$

and thus

$$\gamma = \frac{1}{2} \text{Re}\left\{ \frac{i\Gamma}{2\pi} \left[h \ln\left(\frac{1+G(z_0)}{1+\overline{G(z_0)}}\right) + (1-h) \ln\left(\frac{1-G(z_0)}{1-\overline{G(z_0)}}\right) \right] \right\} = \frac{1}{2} \text{Re}\left\{ \frac{i\Gamma}{2\pi} \ln\left[\left(\frac{1+G(z_0)}{1+\overline{G(z_0)}}\right)^h \left(\frac{1-G(z_0)}{1-\overline{G(z_0)}}\right)^{1-h}\right] \right\}. \tag{16}$$

One can deduce from the mapping of Eq. (1) that

$$\exp\left\{ \pi z_0 + h \ln\left(\frac{h}{1-h}\right) + \ln[2(1-h)] \right\} = (1+G(z_0))^h (1-G(z_0))^{1-h}, \tag{17}$$

and thus

$$\gamma = \frac{1}{2} \text{Re}\left\{ \frac{i\Gamma}{2\pi} \ln\left[\left(\frac{1+G(z_0)}{1+\overline{G(z_0)}}\right)^h \left(\frac{1-G(z_0)}{1-\overline{G(z_0)}}\right)^{1-h}\right] \right\} = \frac{1}{2} \text{Re}\left[\frac{i\Gamma}{2\pi} \ln\left(\frac{e^{\pi z_0}}{e^{\pi \overline{z_0}}}\right) \right] = -\frac{1}{2} \Gamma y_0 \tag{18}$$

regardless of the value of h . As the transverse velocity of the vortex is only significant at the time it is close to the edge, a short duration monopole pulse is generated within the duct at that time.

2.3. The acoustic far field

At low enough Mach number the sound must consist of outwardly propagating one dimensional waves, waves that must match smoothly to outer asymptotics of the essentially incompressible near fields. For $x \rightarrow +\infty$, the sound is

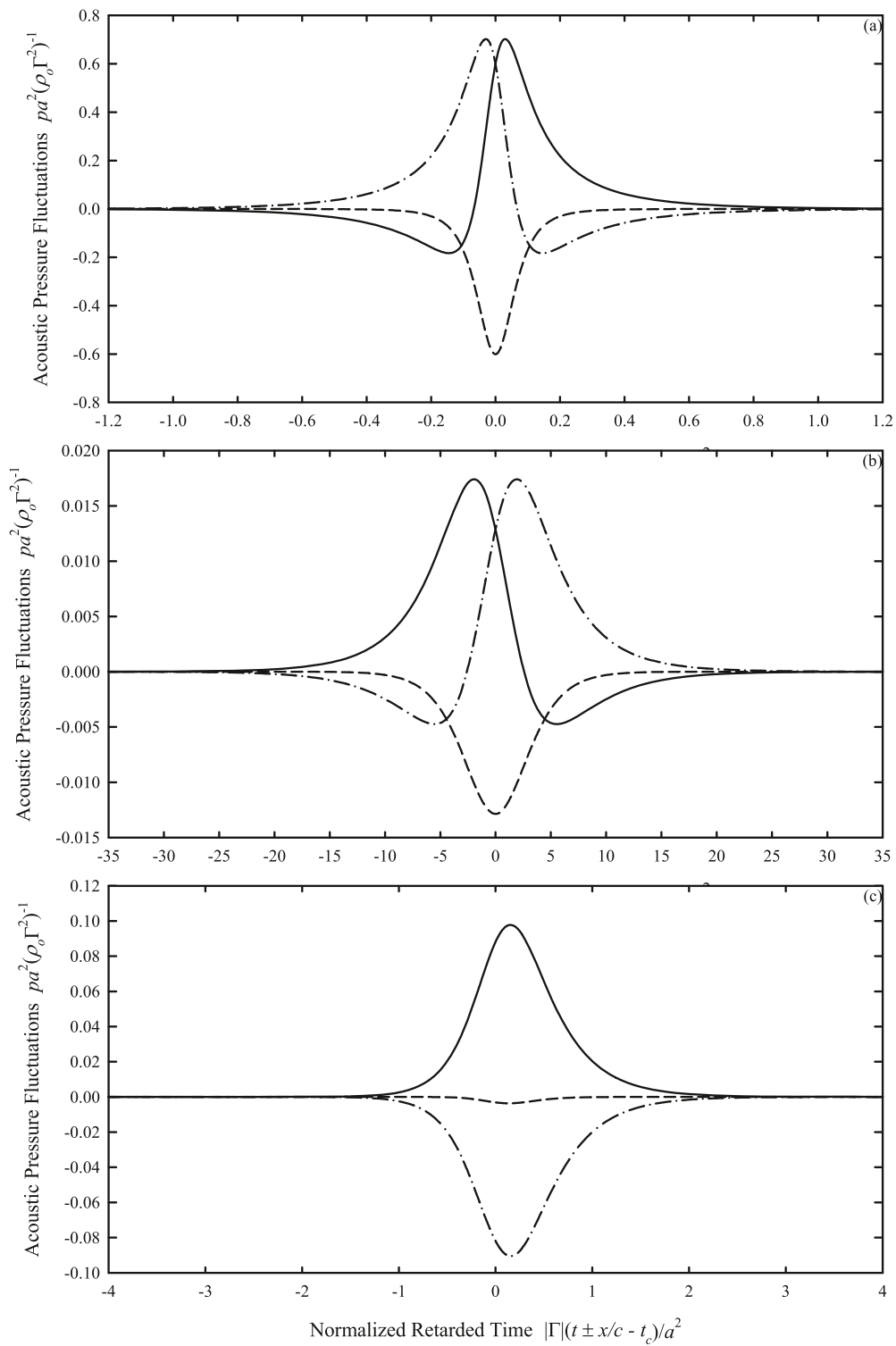


Fig. 5. Far field plane wave pressure fluctuations for $h = 0.5$. (a) $y_i = 0.1, x_i < 0, \Gamma = 1$; (b) $y_i = 0.1, x_i > 0, \Gamma = 1$; (c) $y_i = 0.4, x_i < 0, \Gamma = -1$.: p_o^+ ; p_o^- .

$$p_o \left(t - \frac{x}{c} \right) = -\rho_o \frac{\partial}{\partial t} \gamma \left(t - \frac{x}{c} \right), \tag{19}$$

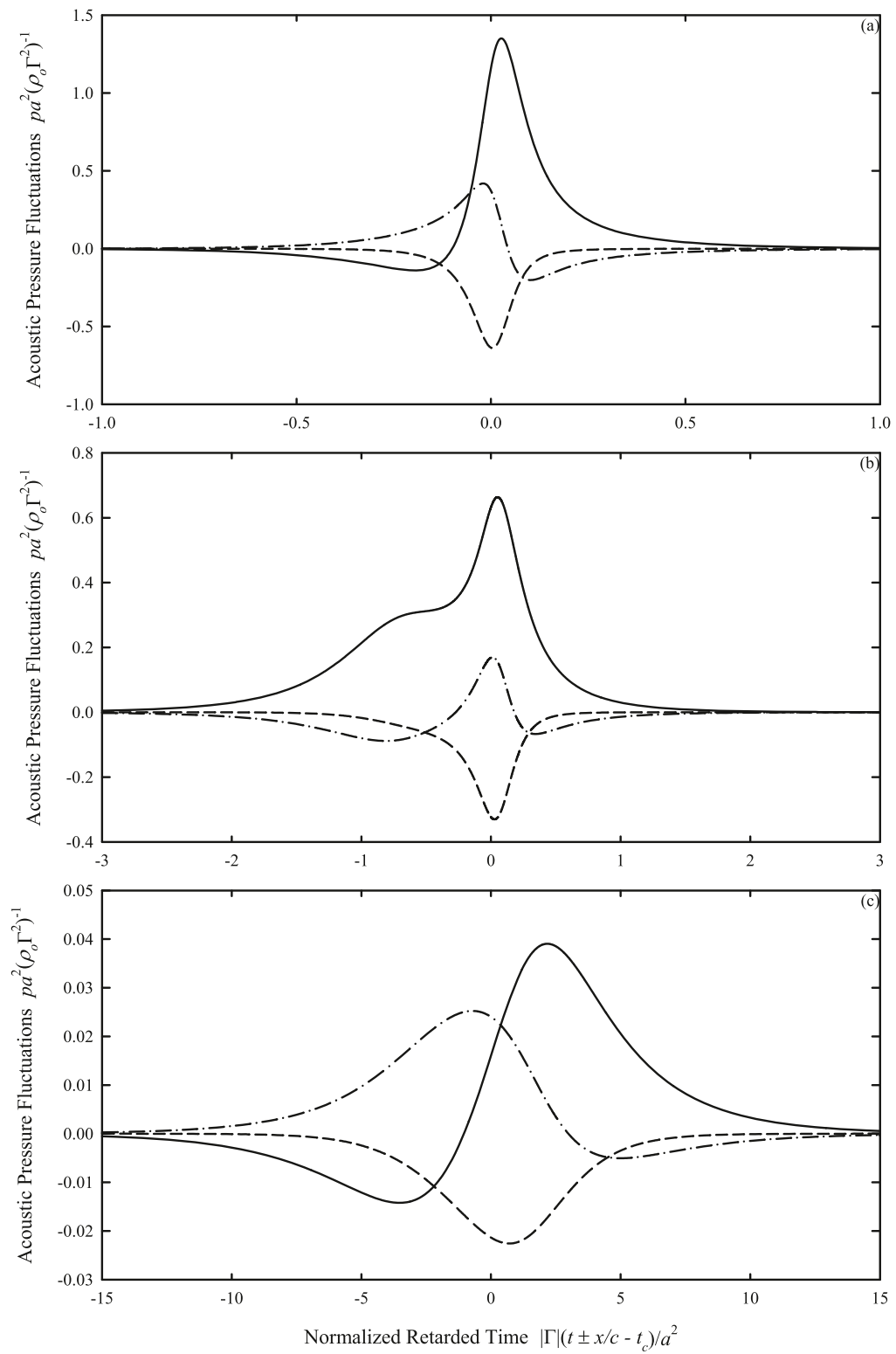


Fig. 6. Far field plane wave pressure fluctuations for $h = 1/3$. (a) $y_i = 0.1, x_i < 0, \Gamma = 1$; (b) $y_i = 0.2, x_i > 0, \Gamma = 1$; (c) $y_i = -0.3, x_i > 0, \Gamma = -1$.: p_0^+ ; $-\cdot-$: p_0^- ; $---$: p_0 .

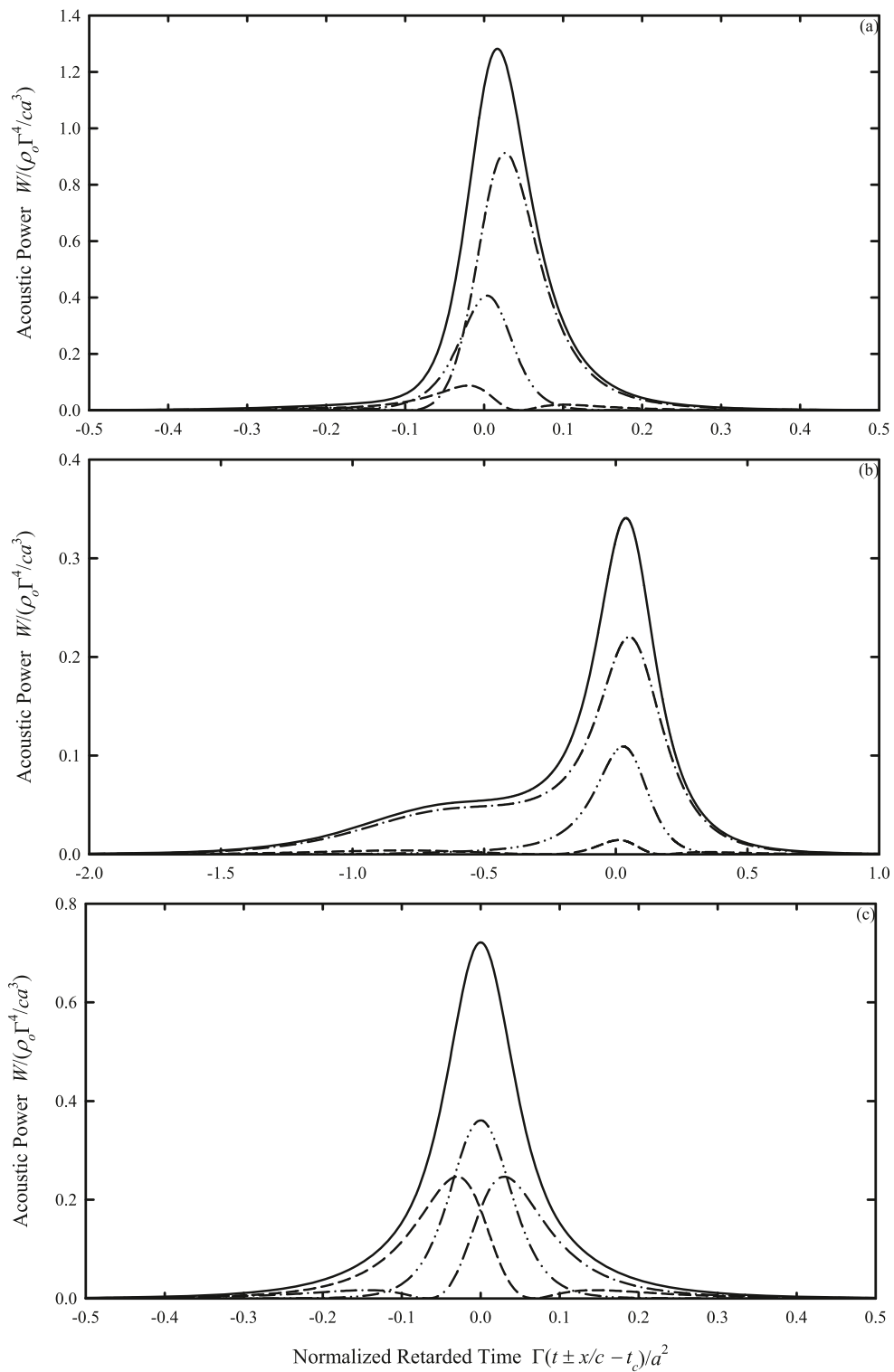


Fig. 7. Examples of time variation of far field sound power radiation. (a) $y_i = 0.1, x_i < 0, \Gamma = 1, h = 1/3$; (b) $y_i = 0.2, x_i > 0, \Gamma = 1, h = 1/3$; (c) $y_i = 0.1, x_i < 0, \Gamma = 1, h = 0.5$.: $y > 0, x \rightarrow -\infty$; $---$: $y < 0, x \rightarrow -\infty$; $- \cdot -$: $x \rightarrow +\infty$: total.

where c is the ambient sound speed. Likewise, the pressure fluctuations as $x \rightarrow -\infty$, are

$$p_o^\pm \left(t + \frac{x}{c} \right) = -\rho_o \frac{\partial}{\partial t} \left\{ \text{Re} \left[-\frac{i\Gamma}{2\pi} \ln \left(\frac{1 \pm G(z_o)}{1 \pm G(z_o)} \right) \right] + \gamma \right\} \tag{20}$$

with an understanding that the right-hand-side of Eq. (20) is evaluated at $t + x/c$. The far field acoustic pressures can in principle be estimated using the Howe’s Green function analogy [1]. However, the required compact Green’s function and the various velocity potentials are not known. Appendix B discusses the plausible use of the Howe’s approach to obtain Eqs. (19) and (20). Further investigation is required before a complete theoretical framework can be sought.

It can be observed from Eqs. (18)–(20) that when the vortex is very close to the edge of the splitter plate, its speed is the highest and the loudest sounds originate there. The sound pressures on the two sides of the splitter plate are concurrent.

Fig. 5(a) illustrates the time variations of the sound pressure for $h = 0.5$ with $y_i = 0.1$ and $x_i < 0$, so that the vortex approaches the edge from the upstream side and the symbol t_c represents the instant the vortex crosses the x -axis. It can be observed from this figure that two upstream compressive waves are produced when the vortex moves across the edge. Since the splitter plate is situated mid-way between the duct walls, it is not surprising to find that in this case the time variations of p_o^+ and p_o^- are mirror images about $t - t_c + x/c = 0$. A rarefaction pulse is produced also at the same time. This pulse tends to weaken the far field sound radiation to the upstream, but the upstream propagating sound pulses remain compressive.

For $y_i = 0.1$ and $x_i > 0$, the vortex approaches the edge from the downstream side. The time variations of far field plane wave pressures are similar to those shown in Fig. 5(a) [see Fig. 5(b)], but with those of p_o^+ and p_o^- interchanged. Compressive pulses and a rarefaction pulse are again produced when the vortex crosses the x -axis. It is also observed that the strengths of the sound waves in Fig. 5(a) are significantly higher than those in Fig. 5(b) because of the much slower speed of the vortex in this case.

Fig. 3 shows that when $|y_i|$ is sufficiently large, the vortex will not turn around the edge but re-adjust its straight path slightly as it moves downstream. A typical example of the sound so produced is illustrated in Fig. 5(c) ($y_i = 0.4$, $x_i < 0$) with t_c representing the instant the vortex moves across the axial location of the edge, $x = 0$. The sound waves radiated into the two sides of the split duct appear to be ‘out-of-phase’ in this case. When y_i is negative, the time variations of the sound waves follow exactly those obtained with $-y_i$, except that the time patterns of p_o^+ and p_o^- are interchanged. Only an insignificantly weak rarefaction pulse is produced in this case because of the very slow transverse vortex motion.

It can be seen from Fig. 5 that the sound pressures are much stronger when the vortex is close enough to the splitter plate to turn around the edge. The magnitudes of p_o^+ and p_o^- are comparable and a monopole-like rarefaction pulse is generated regardless of the vortex’s initial position.

When the plate is offset, the vortex paths are no longer symmetrical about the x -axis (Fig. 4) and no symmetry of the time variations of sound wave pressure about the instant at which the vortex crosses the x -axis can be expected. The pressure variations for the cases where the vortex does not turn around the edge are very similar to those of the symmetrical plate case ($h = 0.5$) and therefore are not presented here.

For $h = 1/3$, $y_i = 0.1$, $x_i < 0$ and $\Gamma > 0$, the turning motion of the vortex near the edge results in a stronger compressive pulse in the upstream upper half plane as shown in Fig. 6(a). The magnitude of the rarefaction pulse is now comparable to that of the pulse in the upstream lower half plane. Though not shown, the time variations of p_o^+ and p_o^- for negative y_i and $x_i < 0$, under which the vortex turns around the edge, are basically similar to those shown in Fig. 6(a) except that p_o^+ and p_o^- are interchanged as in the $h = 0.5$ cases. For $y_i = -0.3$, $x_i < 0$ and $\Gamma < 0$, the vortex continues its propagation upstream but this time with a large change in its traverse position (Fig. 4). The corresponding time variations of sound pressures are very similar to those in Fig. 6(a), except that p_o^+ is always positive; they are not presented.

The vortex with $\Gamma > 0$ approaches the edge from the downstream side for $y_i = 0.2$, $x_i > 0$. The corresponding sound waves are shown in Fig. 6(b). p_o^+ remains positive throughout. For $y_i = -0.3$, the vortex with $\Gamma < 0$ turns back eventually. The pressure patterns resemble very much those in the $h = 0.5$ cases, except that the symmetry is lost [Fig. 6(c)]. The corresponding patterns for $y_i = -0.4$ are even more asymmetrical, but they are not presented.

The results shown in Fig. 6 show again that stronger sound is produced when the vortex turns around the splitter plate edge. One can also infer from this figure that the sound production is a bit biased to regions where the vortex is upstream of the edge [Fig. 6(a) and (b)]. Fig. 7(a) and (b) give some typical examples of the acoustic power (W) variation for $h = 1/3$. At a fixed initial normal distance of the vortex from the splitter plate, the radiated total sound power magnitudes in the offset splitter cases are in general larger than those when $h = 0.5$ (for instance, see Fig. 7c). The acoustic power radiated in the narrower section of the split duct with offset splitter plate is also higher than those in the downstream and in the wider section with the latter is the weakest.

It can be seen from Eqs. (2) and (3) that the potential ϕ scales on Γ and the flow velocity $d\Omega/dz$ on Γ/a . The latter is the characteristic velocity, U , of the present vortex-induced flow. The characteristic time scale is thus the time required for a flow with the speed U to travel over the characteristic length a , which is a^2/Γ . Let $*$ denotes normalized quantity, we then have

$$\phi^* = \frac{\phi}{\Gamma}, \quad t^* = \frac{\Gamma t}{a^2} \quad \text{and} \quad p = -\rho_o \frac{\partial \phi}{\partial t} = -\rho_o \left(\frac{\Gamma}{a} \right)^2 \frac{\partial \phi^*}{\partial t^*}, \tag{21}$$

with ϕ^* and $\partial \phi^*/\partial t^*$ depend only on the normalized locations of the vortex and its image and are independent of the actual values of Γ and a . Since U sets the level of the unsteady pressure, the pressure magnitude scales on the second power of U and the sound intensity of a plane propagating harmonic wave (I), which is the product of its acoustic pressure and acoustic particle velocity [13],

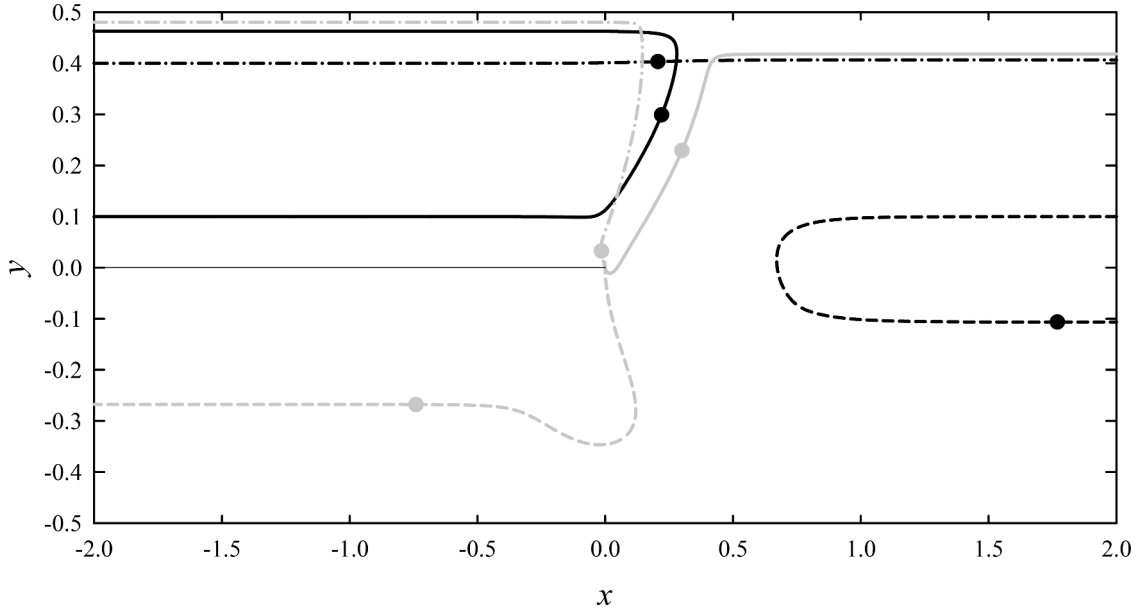


Fig. 8. Vortex flight paths for $h = 0.5$ in the presence vortex shedding at splitter edge.: $y_i = 0.1, x_i < 0, \Gamma = 1$; $---$: $y_i = 0.1, x_i > 0, \Gamma = 1$; $---$: $y_i = 0.4, x_i < 0, \Gamma = -1$. Solid circles: Vortex positions when the first shed vortex becomes a free vortex. Black: initial vortex; grey: first shed vortex. Thin line: splitter plate.

$$I = \frac{p^2}{\rho_o c} = \frac{\rho_o}{c} \left(\frac{\Gamma}{d} \right)^4 \left(\frac{\partial \phi^*}{\partial t^*} \right)^2 \approx \rho_o U^3 M, \quad (22)$$

M being the characteristic Mach number U/c . Comparing this with Crighton's results [4], we see that the confinement of a scattering half plate to the inside of a duct does not alter the radiation efficiency apart from a constant. This is very different from the case of confinement of turbulence that was studied by Davies and Ffowcs Williams [6] where an efficiency increase of M^{-2} is found. They produced the first example showing that flow confined to radiate in a lower dimensional space was a better generator of sound than was the same turbulence in unconfined space. That confined flows make more noise than free flows seemed to be a general result [14]. One naturally wonders whether the acoustical efficiency of edge-scattering flow would be similarly increased by confinement. From what we have done, which is the only example we know of, it seems that it is not. We find that conclusion rather surprising.

3. With vortex shedding

3.1. The unsteady Kutta condition and the vortex paths

The above theoretical vortex dynamic approach gives rise to a fluid velocity singularity at the splitter edge, which does not occur in nature. One of the methods to remove such singularity is to introduce vortex shedding when the initial vortex is still far away from the edge (for instance, Howe [15]). The shed vortex then grows with time in strength and finally detaches from the edge to become a free vortex. A new vortex is shed from the edge at the same time and the cycle repeats.

Let suffix s denotes hereinafter quantity related to the shed vortex when it is still connected to the splitter edge via the feeding vortex sheet, the condition of vanishing fluid velocity at the edge is, as $G(0) = 2h - 1$,

$$\Gamma_s = -\Gamma \frac{|2h - 1 - G(z_s)|^2 \operatorname{Im}(G(z_o))}{|2h - 1 - G(z_o)|^2 \operatorname{Im}(G(z_s))}. \quad (23)$$

Under this condition, this shed vortex is not free to move until Γ_s ceases to grow. The equation governing the motion of this shed vortex was first introduced by Brown and Michael [16], and later Howe [15] proposed an emended version of the equation. However, the formulation of Howe [15] is not designed for confined vortex flow, as the desired streamfunction for fluid motion in the far field in the y -direction is unknown, if not irrelevant. If one considers the whole duct structure, that is the splitter plate and the duct walls, moves along in the y -direction, one possible solution is that the whole fluid in the duct moves at the same speed as the structure. In this case, the Howe's model is reduced to that of Brown and Michael [16]. This is left to further investigation. The model of Brown and Michael [16] is adopted in this study as in Manela and Halachmi [17]. The equation of motion of the shed vortex is

$$\frac{\partial z_s}{\partial t} + \frac{z_s}{\Gamma_s} \frac{\partial \Gamma_s}{\partial t} = \frac{i\Gamma_s}{2\pi} \left[\frac{G''(z_s)}{2G'(z_s)} - \frac{G'(z_s)}{G(z_s) - G(z_s)} \right] + \frac{i\Gamma}{2\pi} \left[\frac{1}{G(z_s) - G(z_o)} - \frac{1}{G(z_s) - G(z_o)} \right] G'(z_s). \quad (24)$$

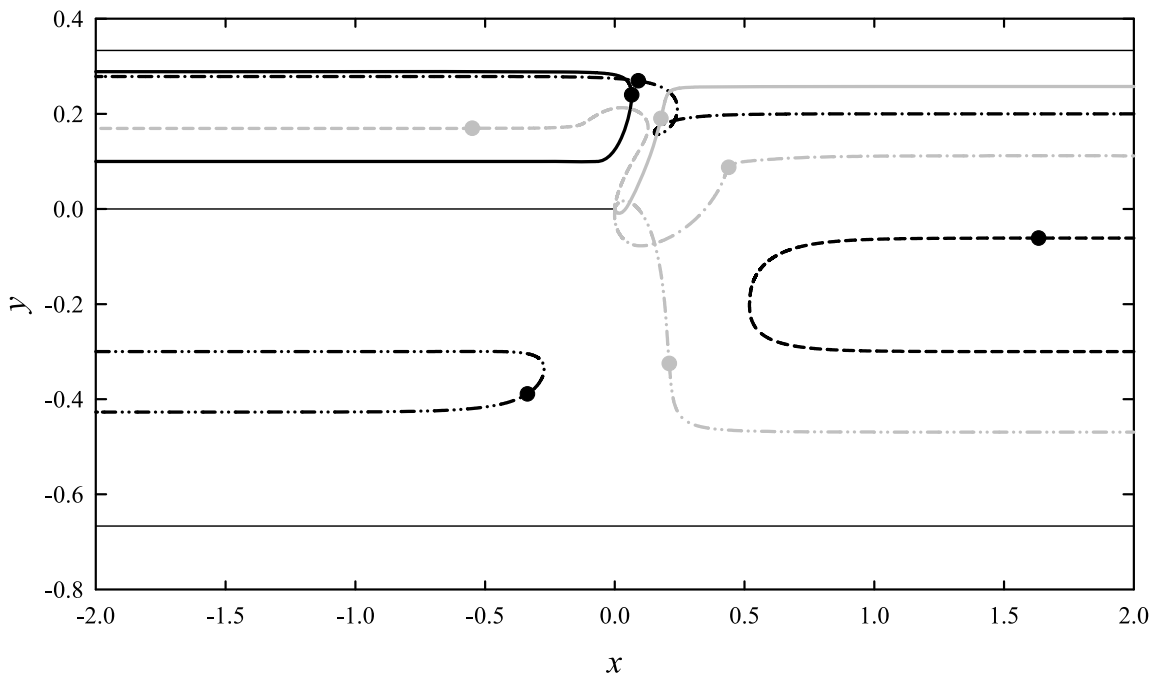


Fig. 9. Vortex flight paths for $h = 1/3$ in the presence vortex shedding at splitter edge.: $y_i = 0.1, x_i < 0, \Gamma = 1$; - - - -: $y_i = -0.3, x_i > 0, \Gamma = -1$; - · -: $y_i = 0.2, x_i > 0, \Gamma = 1$; · · · -: $y_i = -0.3, x_i < 0, \Gamma = -1$. Thin lines: splitter plate and duct walls. Other legends: same as those of Fig. 8.

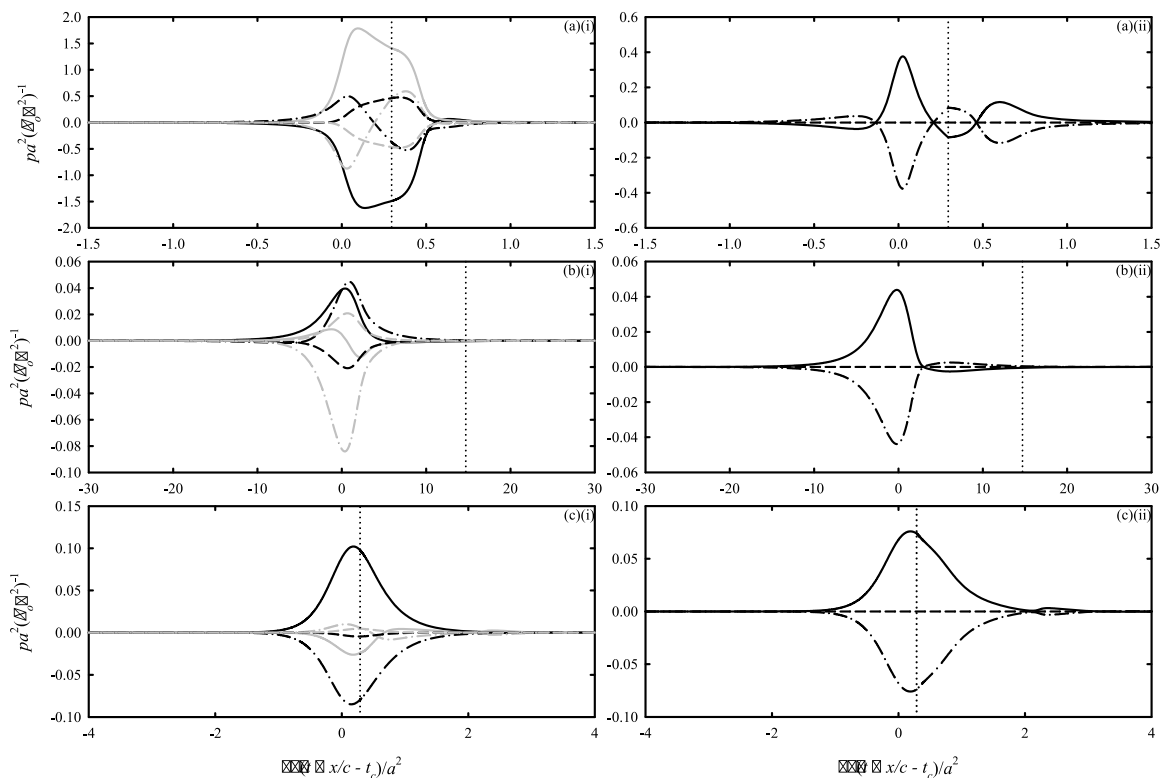


Fig. 10. Far field sound pressure fluctuations for $h = 0.5$ in the presence of vortex shedding. (a) $y_i = 0.1, x_i < 0, \Gamma = 1$; (b) $y_i = 0.1, x_i > 0, \Gamma = 1$; (c) $y_i = 0.4, x_i < 0, \Gamma = -1$. (i) Contributions from initial vortex and shed vortices, Black: initial vortex; grey: shed vortices (combined). (ii) Overall sound pressure fluctuations; p_0^+ : p_0^- ; - - - -: p_0 ; · · · · · : instant at which the first shed vortex detaches from the edge.

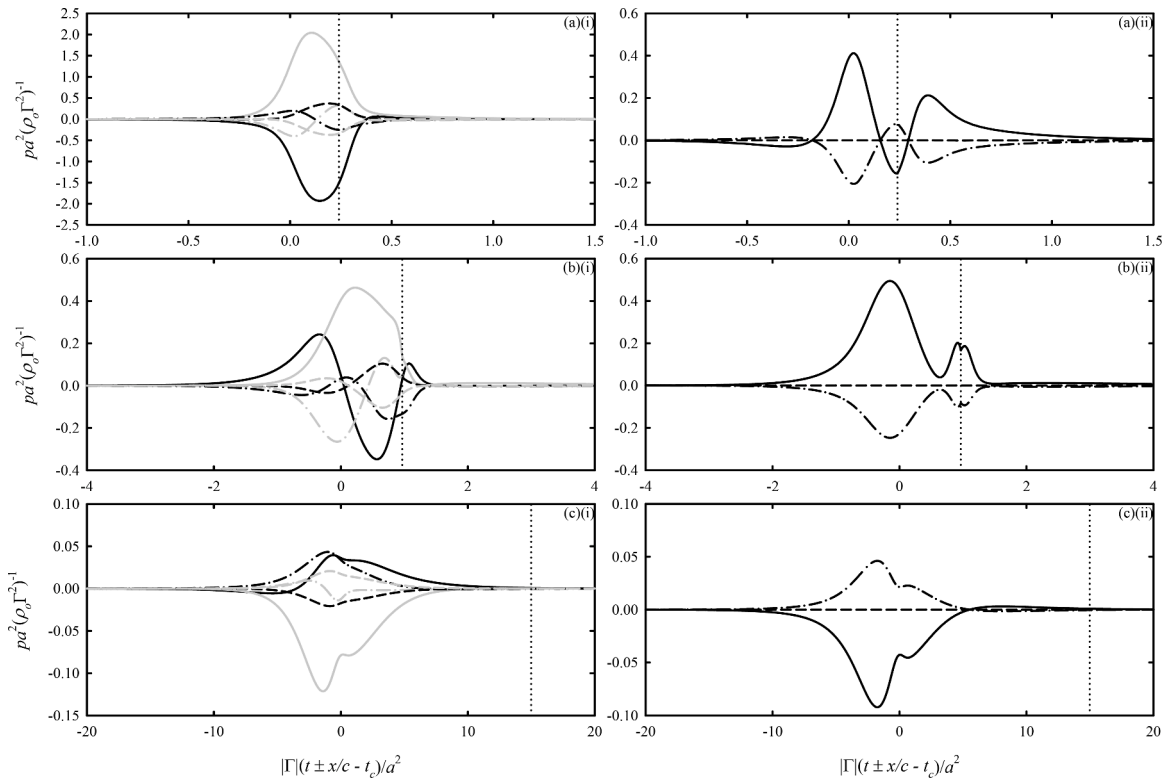


Fig. 11. Far field sound pressure fluctuations for $h = 1/3$ in the presence of vortex shedding. (a) $y_i = 0.1$, $x_i < 0$, $\Gamma = 1$; (b) $y_i = 0.2$, $x_i > 0$, $\Gamma = 1$; (c) $y_i = -0.3$, $x_i > 0$, $\Gamma = -1$. Legends: same as those of Fig. 10.

This shed vortex becomes a free vortex at the instant when $\partial \Gamma_s / \partial t = 0$ (it detaches from the splitter edge). The velocity of the initial vortex is simply

$$\frac{\partial z_o}{\partial t} = \frac{i\Gamma}{2\pi} \left[\frac{G''(z_o)}{2G'(z_o)} - \frac{G'(z_o)}{G(z_o) - \overline{G(z_o)}} \right] + \frac{i\Gamma_s}{2\pi} \left[\frac{1}{G(z_o) - G(z_s)} - \frac{1}{G(z_o) - \overline{G(z_s)}} \right] G'(z_o). \quad (25)$$

Eqs. (23)–(25) can be solved by the fourth order Runge-Kutta method as in Section 2.

The initial strength of the first shed vortex is very weak and its position does not affect the numerical analysis as far as it is close to the splitter edge. In this study, $(x_s, y_s) = (0, -0.01)$ at the beginning of the numerical computation. It is straight-forward to modify Eqs. (23)–(25) to accommodate more free vortices. The modified equations are not presented.

Fig. 8 illustrates some examples of the vortex flight paths for $h = 0.5$, which are in general different from those without vortex shedding. The circles represent the locations of the vortices when the first shed vortices become free to move. It appears that it is not easy for the initial vortex to move across the x -axis in the presence of the vortex shedding. The shed vortex, which has a sense of circulation opposite to that of the initial vortex, tends to wash away the latter when it comes close to the edge. For the case of $y_i = 0.1$, $x_i < 0$, the initial vortex with $\Gamma > 0$ approaches the splitter edge from the upstream and eventually forms a vortex dipole with the shed vortex. Similar phenomenon has been observed in the unconfined splitter case of Howe [15]. The vortex dipole then moves towards the upper duct wall and separate back into individual vortices eventually under the influence of the wall.

For the case of $y_i = 0.1$, $x_i > 0$, the initial vortex with $\Gamma < 0$ approaches the splitter edge from the downstream. The shed vortex moves around the edge and eventually heads towards the upstream under the splitter, while the initial vortex propagates back towards downstream after its engagement with the splitter edge as in the ‘no-vortex-shedding’ case (Fig. 3).

The flight path of the initial vortex with $\Gamma = 1$ initially located at the upstream with $y_i = 0.4$, passes the vertical plane containing the splitter edge and continues its motion straight into the downstream without much affected by the shed vortex (c.f. Fig. 3). The shed vortex is overall weak. It eventually moves near the upper duct wall before it heads upstream, but the initial vortex has already gone very far downstream by that time. The features of the vortex paths in the presence of vortex shedding for $h = 1/3$ are basically similar to those for $h = 0.5$ (Fig. 9). The flight paths are thus not further discussed.

3.2. Far field sound

The far field sound can be estimated in a way similar to that presented in Section 2. In the presence of the shed vortex, it can be shown that

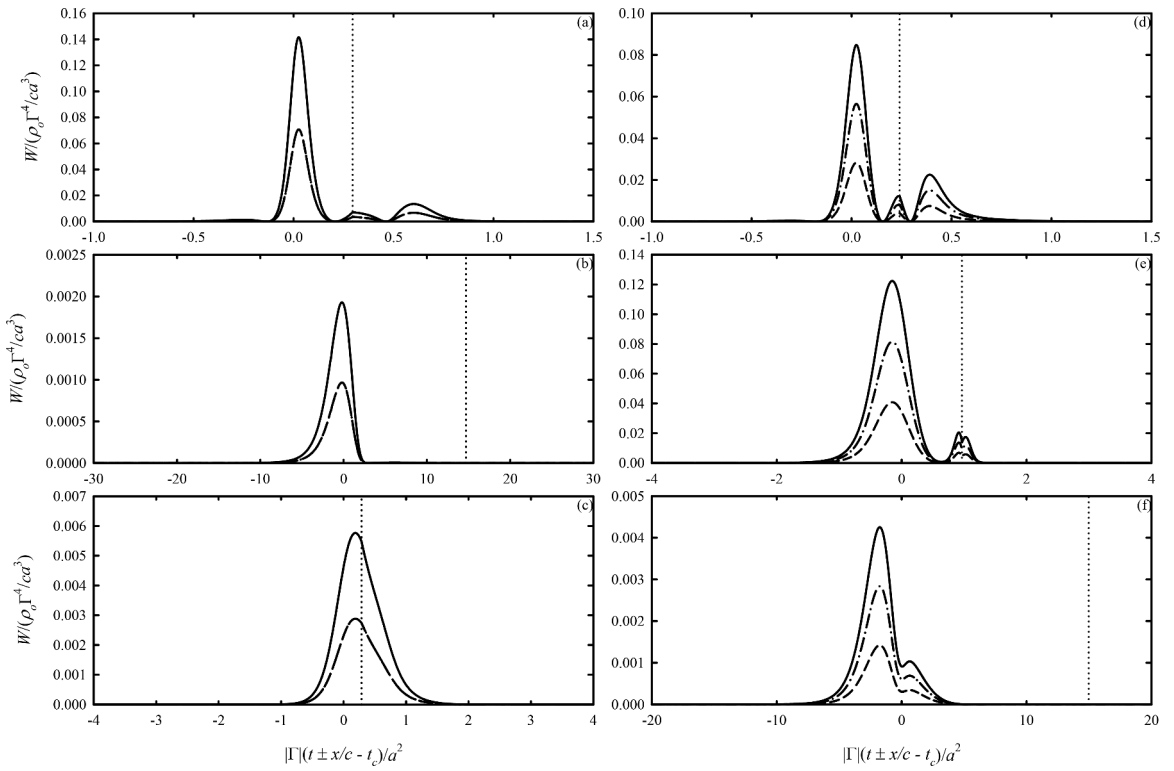


Fig. 12. Sound power radiation in the presence of vortex shedding. $h = 0.5$: (a) $y_i = 0.1$, $x_i < 0$, $\Gamma = 1$; (b) $y_i = 0.1$, $x_i > 0$, $\Gamma = 1$; (c) $y_i = 0.4$, $x_i < 0$, $\Gamma = -1$. $h = 1/3$: (d) $y_i = 0.1$, $x_i < 0$, $\Gamma = 1$; (e) $y_i = 0.2$, $x_i > 0$, $\Gamma = 1$; (f) $y_i = -0.3$, $x_i > 0$, $\Gamma = -1$. $\cdot\cdot\cdot\cdot$: $y > 0$, $x \rightarrow -\infty$; $-\cdot-\cdot-$: $y < 0$, $x \rightarrow -\infty$; total; $\cdot\cdot\cdot\cdot$: instant at which the first shed vortex detaches from the edge.

$$\gamma = -\frac{1}{2}(\Gamma y_o + \Gamma_s y_s), \quad (26)$$

and for $x \rightarrow +\infty$,

$$p_o = -\rho_o \frac{\partial \gamma}{\partial t} = \rho_o \frac{1}{2} \left(\Gamma \frac{\partial y_o}{\partial t} + \Gamma_s \frac{\partial y_s}{\partial t} + y_s \frac{\partial \Gamma_s}{\partial t} \right) \quad (27)$$

with an understanding that all the terms are evaluated at the retarded time $x - t/c$. For $x \rightarrow -\infty$,

$$p_o^\pm \left(t + \frac{x}{c} \right) = \rho_o \frac{\partial}{\partial t} \left\{ Re \left[\frac{i\Gamma}{2\pi} \ln \left(\frac{1 \pm G(z_o)}{1 \pm G(z_o)} \right) \right] + Re \left[\frac{i\Gamma_s}{2\pi} \ln \left(\frac{1 \pm G(z_s)}{1 \pm G(z_s)} \right) \right] - \gamma \right\}, \quad (28)$$

where the right-hand-side of Eq. (28) is evaluated at the retarded time $t + x/c$. Again, Eqs. (26)–(28) can be modified easily to include the effects of more free vortices.

In order to understand the effect of vortex shedding on the sound radiation, the cases considered in Figs. 5 and 6 are re-visited in this section. The corresponding results for $h = 0.5$ and $1/3$ are shown in Figs. 10 and 11, respectively. t_c in the figures denotes the time at which the initial vortex is closest to the splitter edge unless otherwise stated. In these figures, the total contributions from all shed vortices, instead of those of the individual shed vortices, are presented. The subsequently shed vortices are much weaker and thus their individual direct contributions are small. The strongest sound radiation is observed before the first shed vortex detaches from the splitter edge.

Compared with the results shown in Figs. 5 and 6, one can notice that the overall sound intensity is not always reduced in the presence of vortex shedding though the radiation from the initial vortex is counteracted by those of the shed vortices (see Figs. 10a(i), b(i), c(i), 11a(i), b(i) and c(i)). The vortex shedding results in no sound radiation towards the downstream and an acoustic dipole is radiated upstream as shown in the sub-figures (ii) of Figs. 10 and 11. For $h = 0.5$, the sound pressures on the two sides of the splitter far upstream are of the same magnitude and are 180° out-of-phase (Fig. 10). For $h = 1/3$, the magnitude of the far upstream sound pressure in the narrower section of the split duct ($y > 0$) is twice that in the wider split duct section ($y < 0$). The two sound pressures are again 180° out-of-phase. Such dipole patterns can actually be inferred from Eq. (15) when $\partial \gamma / \partial t = 0$. They, together with the vanishing sound pressure downstream, show that there is no horizontal force at the splitter edge in the presence of vortex shedding. The monopole radiation observed previously in Section 2 does not exist here.

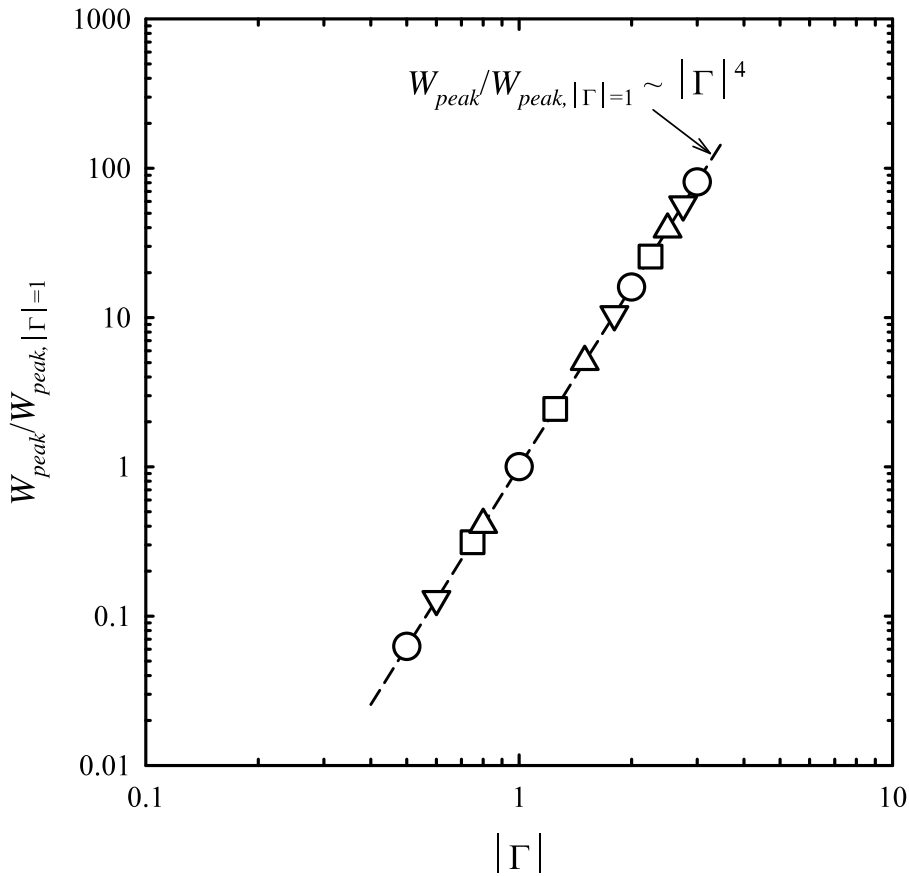


Fig. 13. The scaling law for sound power radiation. \circ : $y_i = 0.1, x_i < 0, \Gamma > 0, h = 1/3$; \square : $y_i = 0.2, x_i > 0, \Gamma > 0, h = 1/3$; \triangle : $y_i = 0.1, x_i < 0, \Gamma > 0, h = 0.5$; \blacktriangledown : $y_i = 0.4, x_i < 0, \Gamma < 0, h = 0.5$; - - - -: the power law.

One can observe by comparing Figs. 5 and 10 that the effect of vortex shedding on the upstream sound radiation depends on the initial location of the initial vortex and how it approaches the splitter edge. Overall sound amplification can be resulted by vortex shedding (Figs. 5b and 10b(ii)). This is not observed in the unconfined splitter case of Howe [15]. These observations are in general found in the corresponding results for $h = 1/3$. Apart from the sound radiated from the shed vortices themselves, these vortices could increase the speed of the initial vortex, resulting in stronger sound radiation.

For the sake of completeness, the overall sound powers radiated by the vortex interactions with the splitter edge included in Figs. 10 and 11 are summarized in Fig. 12. For $h = 0.5$, the upstream sound powers on the two sides of the splitter are the same. For $h = 1/3$, the sound power in the narrower section of the split duct is again twice that in the wider split duct section. Such ratio is not affected by the initial location of the initial vortex (not shown here).

One can observe from Eqs. (22)–(28) that the sound power scaling discussed at the end of Section 2 should apply even in the presence of vortex shedding. This is confirmed in Fig. 13. The total radiated sound power varies with the fourth power of the strength of the initial vortex (and thus the fourth power of the characteristic speed Γ/a).

4. Possible effects of low Mach number mean flows

For the sake of practical interest, it is worthwhile to investigate briefly how the radiated sound will possibly be amplified by the presence of a low Mach number mean flow in the duct. A detailed parametric investigation of mean flow effect is very lengthy. It is left to further study.

For simplicity, we take $h = 0.5$ and the flow speeds far upstream in the split duct sections the same (denoted hereinafter as U_m). The presence of the mean flow over the splitter plate could lead to a shear layer being generated at the splitter edge [1], prohibiting the vortex from crossing the $y = 0$ axis. The implementation of the Kutta condition will then be very different from the one adopted in this study. Thus, Kutta condition is not considered in this preliminary investigation.

The vortex is supposed to be a weak one, such that $U_m > \Gamma/a$. The motion of the vortex can be obtained after adding the complex mean flow potentials [12] into Eq. (2):

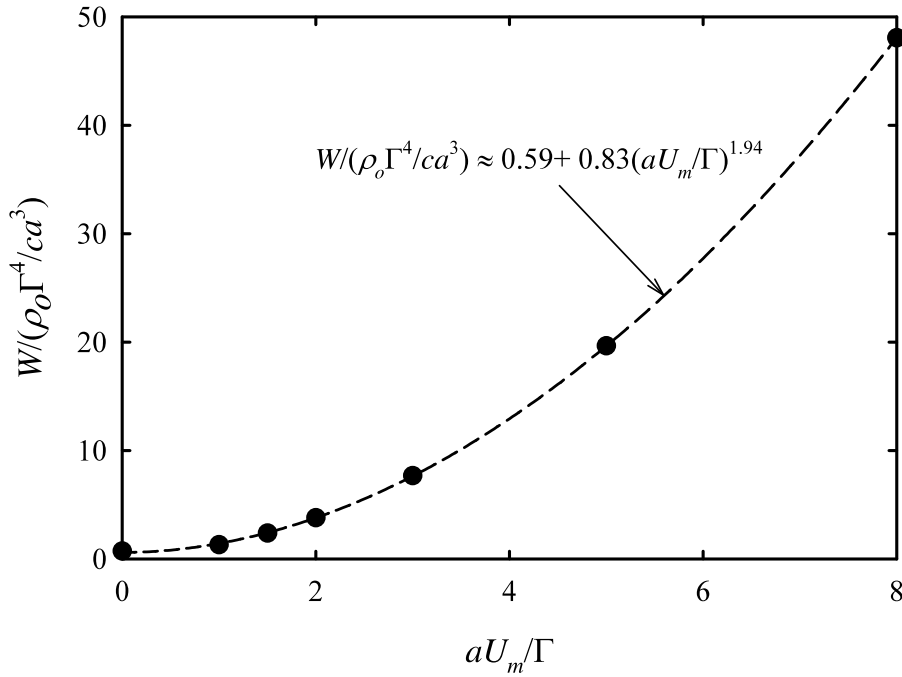


Fig. 14. Indicative effect of low Mach number mean duct flow on overall sound power radiation. $y_i = 0.1$, $x_i < 0$, $\Gamma = 1$, $h = 0.5$. - - -: the regression power law.

$$\Omega = -\frac{i\Gamma}{2\pi} \ln \left[\frac{G(z) - G(z_0)}{G(z) - \bar{G}(z_0)} \right] + \frac{U_m}{\pi} \ln \left[(G(z) - 1)^{1-h} (G(z) + 1)^h \right] + \gamma. \quad (29)$$

We choose the case of $y_i = 0.1$, $x_i < 0$ and $\Gamma = 1$ as an illustrative example. For $U_m > \Gamma/a$, the vortex maintains its path towards the downstream full width duct with its position always above the $y = 0$ axis. There is a slight movement towards the $y = 0$ axis when it propagates across the vertical plane containing the splitter edge (not shown here).

The far field plane wave potentials in the presence of a low Mach number flow satisfy the propagation condition of [18]:

$$\frac{\partial \phi}{\partial x} \Big|_{x \rightarrow \pm\infty} = \mp \frac{1}{c(1 \pm M)} \frac{\partial \phi}{\partial t} \Big|_{x \rightarrow \pm\infty}. \quad (30)$$

One can then estimate the far field acoustic pressure following the procedure given in Section 2. Fig. 14 shows the variation of total radiated sound power with U_m . The sound power appears to rise roughly with the second power of the mean flow speed.

There are many governing parameters for this problem, such as the mean flow speed ratio in the split duct section, the location of the splitter plate, the strength of the vortex relative to the mean flow speeds and etc. A detailed parametric study with Kutta condition imposed is left to further investigation.

5. Conclusions

The sound produced in inviscid fluid, when a vortex filament moves around the edge of a semi-infinite splitter plate inside an infinitely long duct, is studied theoretically by matching the sound to its incompressible near field. Details are given of the vortex trajectories and the time variations of the sound pressure fluctuations within the duct. Both the cases with and without vortex shedding at the splitter edge are investigated.

Without vortex shedding, we find that compressible pulses and a rarefaction pulse are radiated upstream and downstream, respectively, when the vortex turns around the edge of the splitter plate, regardless of the location of the splitter plate. The magnitudes of the sounds are comparable in the two split duct sections provided that the splitter plate is located on the duct centreline. The sound inside the narrower section becomes larger and the sound power radiated into the wider section is in general the weakest when the splitter is offset. There are cases where the vortex is close to the duct wall and it propagates from the upstream, across the transverse plane containing the splitter edge, into the downstream. In these cases, the sound pulses in the upper and lower sections of the split duct section are out-of-phase and the rarefaction pulse downstream is insignificant.

The vortex shedding at the splitter edge removes the flow singularity there and the abovementioned monopole radiation, resulting in a purely dipole radiation into the split duct section. For the splitter plate located in the middle of the duct, the radiated sound powers on the two sides of the splitter plate are the same. For offset splitter plate, the sound intensity in the narrower split duct section is higher than that in the wider section regardless of the way the initial vortex approaches the splitter edge. However, there are cases where

sound is amplified instead of attenuated by vortex shedding. It is also observed that vortex shedding does not have much effect on the sound radiation if the initial vortex is located close to the duct wall in the beginning.

No matter there is vortex shedding or not, we find that the confinement of a sharp edge in flow within a duct does not fundamentally alter the acoustic efficiency of the edge scattering process. We had expected to find an increase in flow noise but find no evidence of this.

Declaration of Competing Interest

None.

Data availability

Data will be made available on request.

Acknowledgments

The idea of this study was conceived during a visit of the author to Professor Ffowcs Williams in his Cambridge University office. That visit and the subsequent visits of the author to Cambridge were supported by grants from the British Council under the Hong Kong / United Kingdom Joint Research Scheme and the Research Grant Council of the Hong Kong Special Administration Region, China (Project No. PolyU5030/00E). The author is very grateful for the advice (on earlier versions of this submission) and encouragement from Professor Ffowcs Williams throughout the past many years.

Appendix A. The matched asymptotic expansion method

As only plane propagating wave will exist in the acoustic far field, the solution of the Helmholtz equation at $x \rightarrow +\infty$ is

$$\phi_o(\omega) = A_o(\omega)e^{-i\omega x/c}, \quad (\text{A1})$$

where ω is the angular frequency, f_o the far field wave potential and A_o its complex magnitude. Under the low frequency and low Mach number condition, the ‘inner’ solution of Eq. (A1) as $\omega x/c \rightarrow 0$ is

$$\phi_o(\omega) = A_o(\omega) \left(1 - \frac{i\omega x}{c} - \left(\frac{\omega x}{c} \right)^2 + \dots \right), \quad (\text{A2})$$

which must match with the ‘outer’ asymptotic of the incompressible flow field potential shown in Eq. (10). Through applying Fourier transform to Eq. (11), one finds

$$A_o(\omega) = \text{F.T.} \left(-\frac{\Gamma}{\pi\beta} \text{Im}[G(z_o)] e^{-\pi x} \cos[(h-1-y)\pi] + \gamma \right) \quad (\text{A3a})$$

$$\text{and } i \frac{\omega}{c} A_o(\omega) = -\text{F.T.}(V), \quad (\text{A3b})$$

where F.T. represents the Fourier transform operation. Therefore

$$V = -\frac{1}{c} \frac{\partial \gamma}{\partial t} \quad (\text{A4})$$

because the first term on the right-hand-side of Eq. (A3a), which represents the incompressible flow field, vanishes as $x \rightarrow +\infty$. The downstream far field plane wave potential in the time domain is thus γ . The above matching procedure can be carried out for the split duct sections at $x \rightarrow -\infty$ to obtain Eq. (14).

In fact, one can also adopt the approach of Cannell and Ffowcs Williams [5] and considers the plane harmonic wave radiation condition in the far field as $x \rightarrow \pm\infty$, which requires

$$\frac{\partial \phi}{\partial x} \Big|_{x \rightarrow \pm\infty} = \mp \frac{1}{c} \frac{\partial \phi}{\partial t} \Big|_{x \rightarrow \pm\infty}. \quad (\text{A5})$$

Matching the condition of Eq. (A5) to the ‘outer’ asymptotic of the incompressible flow field Eqs. (11)–(13) also yields Eq. (14).

Appendix B. The Howe’s analogy [1]

The compact Green’s function approach of Howe [1] can also be used to estimate the sound radiation in the present two-dimensional problem. However, the Green’s function and the required velocity potentials are not currently known. In this appendix, an attempt is made to examine how this Howe’s approach could be applied with reference to the properties of the complex

vortex potential given in Eq. (2). Further investigation is required to work out the approach analytically.

We first observe that the present low Mach number condition ensures plane wave propagation in the locations far away from the splitter edge. The corresponding low frequency plane wave Green's function G is,

$$\mathbb{G}(\mathbf{x}, \mathbf{y}, t - \tau) = \frac{c}{2w} H\left(t - \tau - \frac{|\mathbf{x} - \mathbf{Y}|}{c}\right), \tag{B1}$$

where H is the Heaviside step function, w the duct width, $\mathbf{x} (x_1, x_2)$ and $\mathbf{y} = (y_1, y_2)$ far field and near field distances, respectively, (the suffices 1 and 2 denote quantities in the longitudinal and transverse direction, respectively) and \mathbf{Y} the Kirchhoff vector. In the present plane wave propagation in the longitudinal direction,

$$\mathbf{Y} = (y_1 - \varphi, y_2) \tag{B2}$$

where φ is an instantaneous velocity potential due to motion of solid surfaces as described in Howe [11]. The sound in the far field is given by

$$p(x, t) = -\rho_o \int \Gamma(\hat{y}_3 \times \mathbf{v}) \cdot \nabla \mathbb{G} d\tau, \tag{B3}$$

where \hat{y}_3 is the unit vector in the spanwise direction. For plane wave propagation, one obtains as $x_1 \rightarrow \pm\infty$,

$$\nabla \mathbb{G} = \frac{c}{2} \nabla H\left(t - \tau - \frac{|\mathbf{x} - \mathbf{Y}|}{c}\right) = \frac{x_1}{2|\mathbf{x}|} \delta\left(t - \tau - \frac{|\mathbf{x}|}{c}\right) \nabla Y_1. \tag{B4}$$

The incompressible velocity potential giving a unit speed uniform flow in the duct at $x_1 \rightarrow +\infty$, is just y_1 . Also, the vortex motion results in vanishing potential at $x_1 \rightarrow +\infty$. The corresponding Kirchhoff vector is

$$\mathbf{Y}_{+\infty} = y_1 \Rightarrow \varphi_{+\infty} = 0 \text{ and } \nabla \mathbf{Y} = \hat{y}_1. \tag{B5}$$

The sound at $x_1 \rightarrow +\infty$ is

$$p_{+\infty} = -\frac{1}{2} \rho_o \Gamma \int (\hat{y}_3 \times \mathbf{v}) \cdot \hat{y}_1 \delta\left(t - \tau - \frac{|\mathbf{x}|}{c_o}\right) d\tau = \frac{1}{2} \rho_o \Gamma \left[\frac{\partial y_2}{\partial t} \right]_{z_o}, \tag{B6}$$

where the term in the square parenthesis is evaluated at the retarded time $t - |\mathbf{x}|/c$. Eq. (B6) is exactly the same as Eq. (19), which is independent of h . It should be noted that γ in Eq. (2) represents a plane wave monopole radiation to $x_1 \rightarrow \pm\infty$.

The condition at $x_1 \rightarrow -\infty$ is complicated by the presence of the splitter plate at $y_2 = 0$. The compact Green's function appears very much not straight-forward and its derivation is left to further studies. However, the potential given in Eq. (B5) appears to be a general solution regardless of y_2 . As we are considering a uniform upstream moving flow because of the abovementioned monopole radiation, the corresponding far field acoustic pressure is

$$p_{-\infty} = \frac{x_1}{2|\mathbf{x}|} \rho_o \Gamma \int (\hat{y}_3 \times \mathbf{v}) \cdot \hat{y}_1 \delta\left(t - \tau - \frac{|\mathbf{x}|}{c_o}\right) d\tau = \frac{1}{2} \rho_o \Gamma \left[\frac{\partial y_2}{\partial t} \right]_{z_o}, \tag{B7}$$

which is uniform over the cross section of the whole split duct section.

The first term in the right-hand-side of Eq. (2) results in a vanishing potential far downstream of the splitter edge and the sound so radiated goes only into the split duct sections (one-sided). The corresponding Green's function for $x_2 > 0$ at $x_1 \rightarrow -\infty$ is

$$\mathbb{G}_{-\infty}^+ = \frac{c}{h} H\left(t - \tau - \frac{|\mathbf{x} - \mathbf{Y}_{-\infty}^+|}{c}\right). \tag{B8}$$

The Kirchhoff vector represents a velocity potential which gives a unit flow at large distance from the edge and fits the boundary conditions of the current problem. One of the possible solutions is

$$Y_{-\infty,1}^+ = \frac{h}{\pi} \text{Re}(\log(G(z) + 1)). \tag{B9}$$

Let Φ be the corresponding complex potential, $\Phi = \frac{h}{\pi} \log(G(z) + 1)$ and

$$\frac{d\Phi}{dz} = \frac{h}{\pi} \frac{d}{dz} \log(G(z) + 1) = \frac{h}{\pi} \frac{G'(z)}{G(z) + 1} = \frac{\partial Y_{-\infty,1}^+}{\partial y_1} - i \frac{\partial Y_{-\infty,1}^+}{\partial y_2}, \tag{B10}$$

where $G'(z) = dG/dz$ and use has been made of the Cauchy-Riemann principle. Therefore,

$$\nabla Y_{-\infty,1}^+ = \text{Re}\left(\frac{h}{\pi} \frac{G'(z)}{G(z) + 1}\right) \hat{y}_1 - \text{Im}\left(\frac{h}{\pi} \frac{G'(z)}{G(z) + 1}\right) \hat{y}_2. \tag{B11}$$

The corresponding far field acoustic pressure is

$$\begin{aligned}
p_{-\infty,\Omega}^+ &= \frac{\rho_o \Gamma}{h} \left[(\hat{y}_3 \times \mathbf{v}) \cdot \left(\operatorname{Re} \left(\frac{h}{\pi} \frac{G'(z)}{G(z)+1} \right) \hat{y}_1 - \operatorname{Im} \left(\frac{h}{\pi} \frac{G'(z)}{G(z)+1} \right) \hat{y}_2 \right) \right]_{z_o} = -\frac{\rho_o \Gamma}{\pi} \left[\frac{\partial y_2}{\partial t} \operatorname{Re} \left(\frac{G'(z)}{G(z)+1} \right) + \frac{\partial y_1}{\partial t} \operatorname{Im} \left(\frac{G'(z)}{G(z)+1} \right) \right]_{z_o} \\
&= -\frac{\rho_o \Gamma}{\pi} \left[\operatorname{Im} \left(\frac{G'(z)}{G(z)+1} \frac{\partial z}{\partial t} \right) \right]_{z_o},
\end{aligned} \tag{B12}$$

where again the term in square parenthesis is evaluated at the retarded time $t - |\mathbf{x}|/c$. The total far field acoustic pressure in the upper split duct section is

$$p_{-\infty,o} + p_{-\infty,\Omega}^+ = \frac{1}{2} \rho_o \Gamma \left[\frac{\partial y_2}{\partial t} \right]_{z_o} - \frac{\rho_o \Gamma}{\pi} \left[\operatorname{Im} \left(\frac{G'(z_o)}{G(z_o)+1} \frac{\partial z_o}{\partial t} \right) \right], \tag{B13}$$

which is exactly Eq. (20) after some algebra. Likewise for $x_2 < 0$, the Green's function and one possible velocity potential for $x_2 < 0$ at $x_1 \rightarrow -\infty$ is

$$\mathcal{G}_{-\infty}^- = \frac{c}{1-h} H \left(t - \tau - \frac{|\mathbf{x} - \mathbf{Y}_{-\infty}^-|}{c} \right) \text{ and } Y_{-\infty,1}^- = \frac{1-h}{\pi} \operatorname{Re}(\log(G(z) - 1)) \tag{B14}$$

respectively. The total far field acoustic pressure in the lower split duct section is

$$p_{-\infty,o} + p_{-\infty,\Omega}^- = \frac{1}{2} \rho_o \Gamma \left[\frac{\partial y_2}{\partial t} \right]_{z_o} - \frac{\rho_o \Gamma}{\pi} \left[\operatorname{Im} \left(\frac{G'(z_o)}{G(z_o)-1} \frac{\partial z_o}{\partial t} \right) \right], \tag{B15}$$

which is the same as Eq. (20).

This appendix shows that one could reproduce the far field acoustic pressures obtained by the matching asymptotic expansion using Howe's compact Green's function approach with the known properties of the complex vortex potential. Further investigation is needed to provide a formal theoretical proof of the working.

References

- [1] M.S. Howe, *Theory of Vortex Sound*, Cambridge University Press, Cambridge, 2003.
- [2] J.E. Ffowcs Williams, L.H. Hall, Aerodynamic sound generation by turbulent flow in the vicinity of a scattering half-plate, *J. Fluid Mech.* 40 (1970) 657–670.
- [3] D.G. Crighton, F.G. Leppington, On the scattering of aerodynamic noise, *J. Fluid Mech.* 46 (1971) 577–597.
- [4] D.G. Crighton, Radiation from vortex filament motion near a half plane, *J. Fluid Mech.* 51 (1972) 357–362.
- [5] P. Cannell, J.E. Ffowcs Williams, Radiation from line vortex filaments exhausting from a two-dimensional semi-infinite duct, *J. Fluid Mech* 58 (1973) 65–80.
- [6] H.G. Davies, J.E. Ffowcs Williams, Aerodynamic sound generation in a pipe, *J. Fluid Mech.* 32 (1968) 765–778.
- [7] D.G. Crighton, Airframe noise, *Aeroacoust. Flight Veh. Theory Pract.* 1 (1995) 391–447.
- [8] M.S. Howe, Sound produced by a vortex interacting with a cavitating wake, *J. Fluid Mech.* 543 (2005) 333–347.
- [9] A. Manela, L. Huang, Point vortex model for prediction of sound generation by a wing with flap interacting with a passing vortex, *J. Acoust. Soc. Am.* 133 (2013) 1934–1944.
- [10] H. Abou-Hussein, A. De Benedicts, N. Harrison, M. Kim, M.A. Rodrigues, F. Zagadou, M.S. Howe, Vortex-surface interaction noise: a compendium of worked examples, *J. Sound Vib.* 252 (2002) 883–918.
- [11] D.G. Crighton, The Kutta conditions in unsteady flow, *Ann. Rev. Fluid Mech.* 17 (1985) 411–445.
- [12] R.V. Churchill, J.W. Brown, *Complex Variables and Applications*, McGraw-Hill, Singapore, 1984.
- [13] L.E. Kinsler, A.R. Frey, A.B. Coppens, J.V. Sanders, *Fundamentals of Acoustics*, 4th ed., Wiley, New York, 2000.
- [14] J.E. Ffowcs Williams, Hydrodynamic noise, *Ann. Rev. Fluid Mech.* 1 (1969) 197–222.
- [15] M.S. Howe, Emendation of the Brown & Michael equation, with application to sound generation by vortex motion near a half-plane, *J. Fluid Mech.* 329 (1996) 89–101.
- [16] C.E. Brown, W.H. Michael, Effect of leading edge separation on the lift of a delta wing, *J. Aerosp. Sci.* 21 (1954) 690–706.
- [17] A. Manela, M. Halachmi, Mechanisms of sound amplification and sound reduction in the flapping flight of side-by-side airfoils, *J. Sound Vib.* 346 (2015) 216–228.
- [18] J.E. Ffowcs Williams, M.S. Howe, The generation of sound by density inhomogeneities in low Mach number nozzle flows, *J. Fluid Mech.* 70 (1975) 605–622.